eismic Behaviou Imp ovement of teel-Conc ete Composite F ames Based on teel pi al-Confined labs

Nicola Troiano, Marco Fasan, Chiara Bedon, and Claudio Amadio(✉)

University of Trieste, Trieste, Italy
amadio@units.it

Abst act. The use of continuous spiral reinforcements can be an efficient solution for the seismic performance improvement of reinforced concrete members. Several literature studies confirm their positive confinement effects especially for concrete columns, where typical benefits take the form of enhanced ductility and energy dissipation capacity.

In this paper, the attention is focused on steel-concrete composite frames, where the study of both joint and slab detailing can involve several design challenges. Steel spirals are thus introduced for the seismic reinforcement of concrete slabs. Based on literature documents and a set of parametric Finite Element (FE) numerical analyses, selected configurations of technical interest are explored. As a first key step, the compressive response of concrete slabs with confining steel spirals is discussed, with a focus on local and global effects.

Keywo ds: Stee-concrete composite frames · Spiral reinforcement · Slab confinement · Finite Element (FE) numerical analysis

nt oduction

se of steel spiral-based confinement techniques can be strongly efficient fo rcement of concrete load-bearing members. Literature studies show that s e beneficial to increase the axial capacity of columns [1, 2]. However, ete composite systems are characterized by high design complexity [3] and re the use of expensive numerical/experimental analyses, see [4, 5] and Fig this paper, a novel application of steel spirals to steel-concrete composite fr essed with the support of FE analyses carried out in ABAQUS. The study ts a first outcome for the optimization of an enhanced reinforcement techn nal effect of steel spirals on the compressive behaviour of concrete slabs is n issue to address for steel-concrete composite systems under seismic loads nted parametric results show that a minimum amount of steel spirals can acti and-tie resistant mechanism for the slab, and thus allow to strongly increas racked resistance, stiffness and overall ductility of traditional slabs.

Mazzolani et al. (Eds.): STESSA 2022, LNCE 262, pp. 597–605, 2022.
doi.org/10.1007/978-3-031-03811-2_64

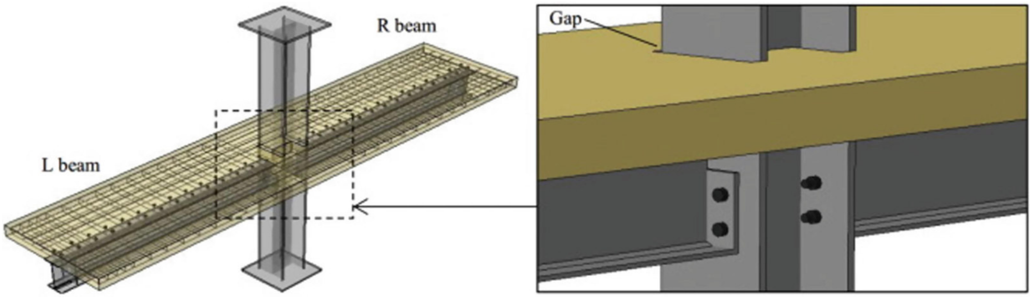

Fig. 1. Reference steel-concrete composite frame and joint detail.

Numerical Anal sis

.1 Original S stem

The reference specimen is derived from the experimental investigation presented in [6]. The layout agrees with Fig. 2 and includes a steel column (HEB280) and a trapezoidal slab (100 mm in thickness). A set of 5ϕ12 tension bars and a 150 × 150 ϕ8 mesh, with 4ϕ8 stirrups in the column region, are used for concrete (R_{ck} = 35 MPa). An additional 40 mm thick opening is placed in front of the column stub, for the de-activation of the resistant mechanism 1 (Eurocode 8, Annex C). Moreover, the boundary conditions of the slab specimen take the form of two simply supports (280 mm in width). The extension of supports, as well as the 45° inclination for the upper part of the slab, are derived from the original setup discussed in [6], where it was designed to force the complete development of the resistant mechanism 2 for the examined system. The vertical compressive load is imposed to the top face of the steel column, while monitoring the relative vertical deformation of the slab.

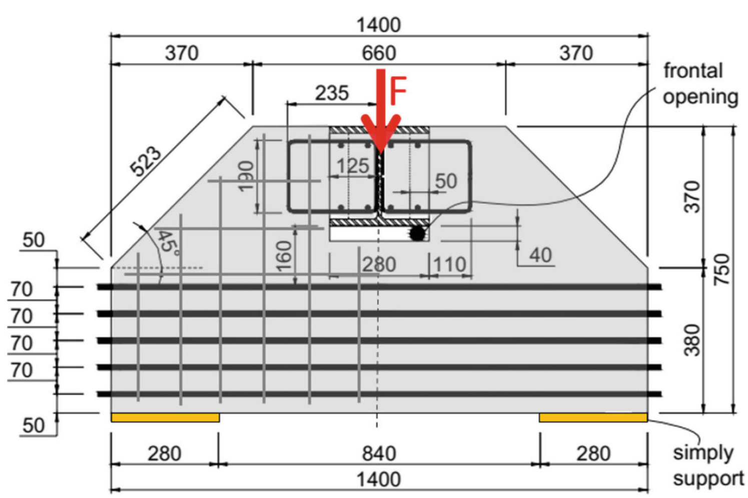

Fig. . Unreinforced slab specimen for the compressive performance assessment: in evidence, the nominal geometry (dimensions in mm) and the test setup (front view).

In presence of the resistant mechanisms 2 only like for the slab in Fig. 2, the Eurocode 8 requires that the transversal cross-section A_T of the tension bars would be minimum equal to:

$$A_T \geq A_{T,2,lim} = 0.5 \frac{F_{Rd,2}}{f_{sd}} \tag{1}$$

with $F_{Rd,2}$ and f_{sd} the design resistance of the mechanism and the yielding strength of anchored steel bars. In this paper, such a design issue is addressed with the use of additional steel spirals that can interact with transversal tension bars and activate a strut-and-tie resisting mechanism, with the consequent effect of a high confinement for the slab.

2.2 Confinement of the Concrete Slab with Steel Spirals

For the purpose of this study, the reference system is derived from the nominal geometry in Fig. 2. Various configurations are taken into account for the introduction of steel spirals (i.e., number, length, diameter, inclination), with the aim to connect the column/load region with the bottom tension bars. A schematic example is shown in Fig. 3 and gives evidence of the expected working mechanism. Worth to note that the solution can involve circular or rectangular stirrups/welded fabrics as in Fig. 3.

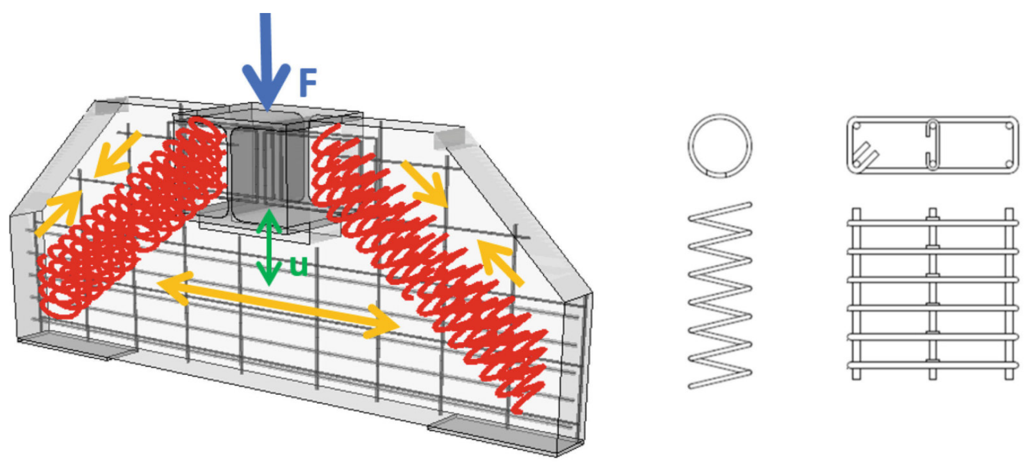

Fig. 3. Response of the slab with steel spirals and strut-and-tie mechanism, and possible arrangement of spirals.

The expected confinement effects are in fact directly proportional to the amount of steel and the confined concrete volume, given that the lateral confinement pressure is:

$$\sigma_l \propto \frac{A_{st}}{s \cdot A_{conf}} \tag{2}$$

with A_{st}, A_{conf} the resisting section of steel and confined concrete respectively, and s the pace of spirals as in Fig. 3. Further, Eq. (2) can be adapted to groups of spirals (with geometrical parameters defined according to Fig. 4), where:

$$\sigma_l = \sqrt{\frac{n_x n_y}{b_x b_y}} \cdot \frac{A_{st} f_{sk}}{s} \tag{3}$$

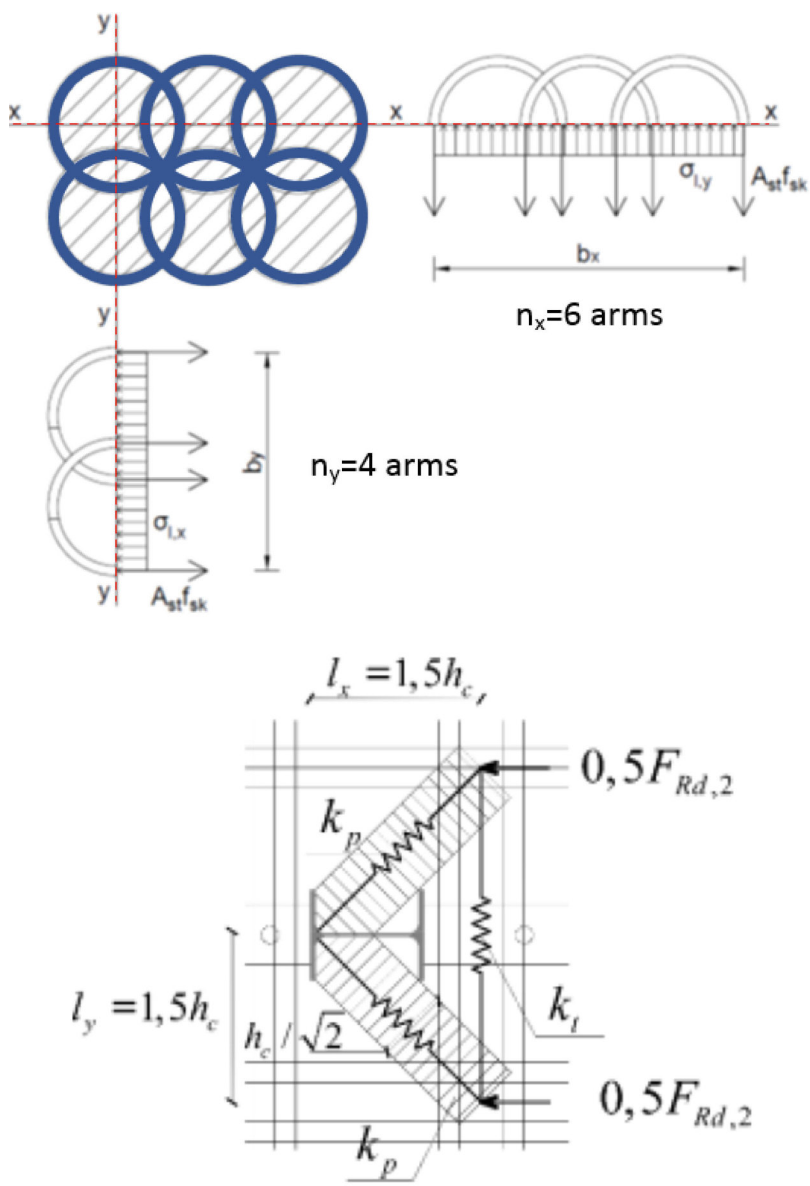

(a)

(b)

Fig. 4. Schematic equilibrium for the confinement effect of spirals: (a) geometrical parameters and (b) activation of the resistant mechanism.

2.3 Numerical Modelling

The numerical analysis is carried out in ABAQUS [7], in the form of nonlinear dynamic simulations with a quasi-static deformation regime. The typical geometry in Figs. 2 and 3 is reproduced in the form of solid brick elements, while mono-dimensional B31 type beam elements are used for the steel tension bars and stirrups. The steel spirals for the confinement of the slab (circular type, 8 mm in nominal diameter) are also described with solid brick elements. Further, to avoid local damage effects at the symmetry conditions, finally, the full geometry is reproduced.

The overall modelling approach takes inspiration from [4, 5], both in terms of geometrical and mechanical characterization of the involved load-bearing components. For the materials, an equivalent elastic-plastic constitutive law is used for all the steel components. The "Concrete Damaged Plasticity" material model is also used for concrete. For all the constitutive laws in tension, compression or damage stage, nominal material properties are considered, based on the resistance classes defined in [6], and the reference empirical models discussed in [4, 5].

A variable mesh pattern was used for the discretization of brick elements, with an edge size in the range from 8 mm to 20 mm maximum. The mesh pattern was chosen so as to capture any local fracture in the slab, through the loading stage. Most of the mesh pattern (90%) consisted of hexahedral solid elements, while a minimum part of wedge elements was used in the corner regions, to respect the geometrical shape of the slab. The final result consisted in 130,000 elements and 420,000 DOFs.

The "embedded" constraint is used to provide the structural coupling between the slab and the steel members, both in the case of the base rebars and spirals. The vertical compressive load is then introduced in the form of a displacement-controlled setup, with a monotonic vertical displacement that is applied to the top surface of the HEB280 column, while monitoring the vertical reaction forces at the supports. In the same way, the propagation of maximum stress and strain peaks in al the FE components is continuously monitored through the analysis. Further, a special care is spent for the analysis of the damage mechanism, including both the possible yielding of steel rebars but also the progressive fracture and cracking of the slab.

3 Results

3.1 Load-Displacement Response

At first, the analysis of parametric numerical results is carried out by comparison of the collected compressive load and vertical displacements of the tested configurations. Figure 5 collects some of the most relevant configurations for the numerical study, with the base, unreinforced slab that is plotted as a base reference for the analysis of local and global effects due to spirals. Moreover, Fig. 5 gives evidence of the first yielding for the tension bars. As shown, the presence of steel spirals results in marked increase of global compressive capacity of the slab. The initial elastic stiffness minimally increases with the number of steel spirals. More interestingly, the post-cracked stiffness and resistance increases largely and is characterized by a more stable and ductile performance of the slab. On the other side, the more the steel spirals are introduced, and the more premature can be the first yielding of the tension bars, thus requiring an optimal design of all the mechanism components.

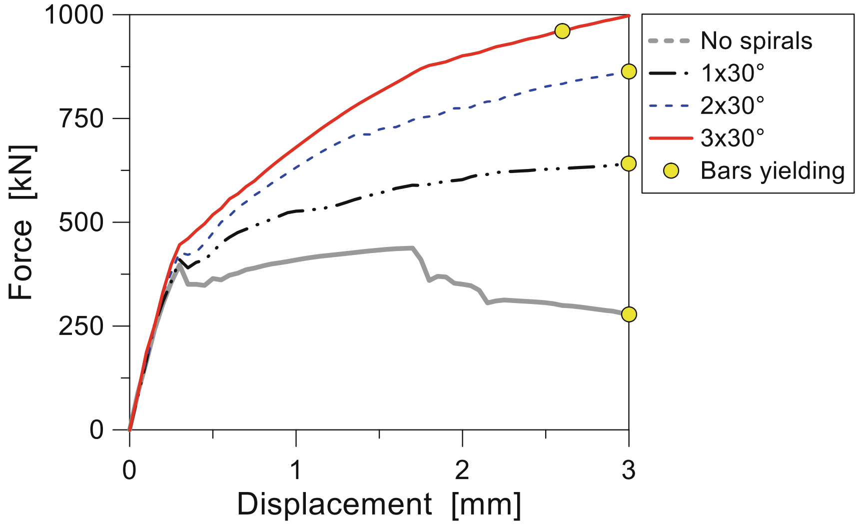

Fig. 5. Load-displacement response of the slab with various arrangements of steel spirals (ABAQUS).

As far as the steel spirals are not properly arranged in terms of inclination for the desired mechanism, the benefits can fully vanish and minimize the potential of the approach. An example is shown in Fig. 6, where it is possible to see that the 2 spirals with 45° of inclination roughly provide the same resistance increase of a single spiral with higher inclination ($1 \times 30°$).

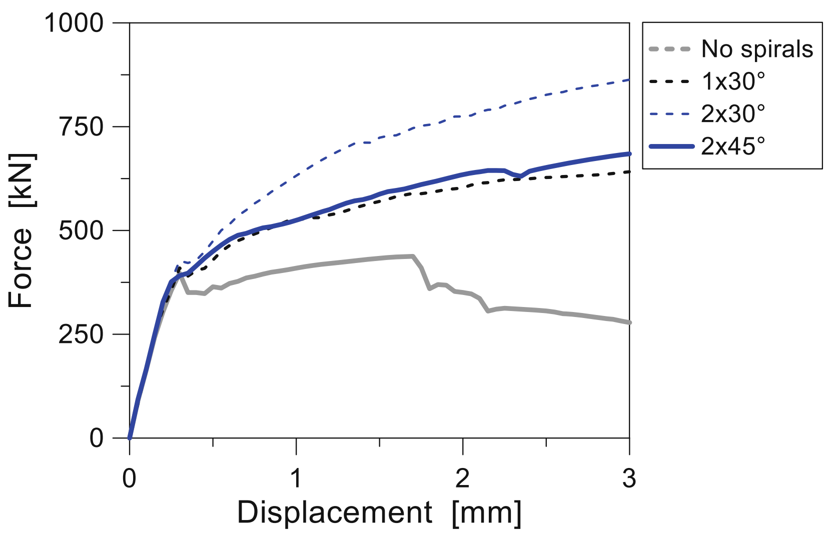

Fig. 6. Load-displacement response of the slab with various arrangements of steel spirals (ABAQUS).

3.2 Qualitative Stress and Damage Evolution

The tensile stress evolution and damage propagation/cracking in the concrete slab can be efficiently investigated in terms of vectorial stress patterns and DAMGET non-dimensional parameter. Figures 7 and 8 present respectively the evolution of stress peaks and tensile cracks for the slab without spirals, as observed at a vertical deformation of 1 mm or 2 mm.

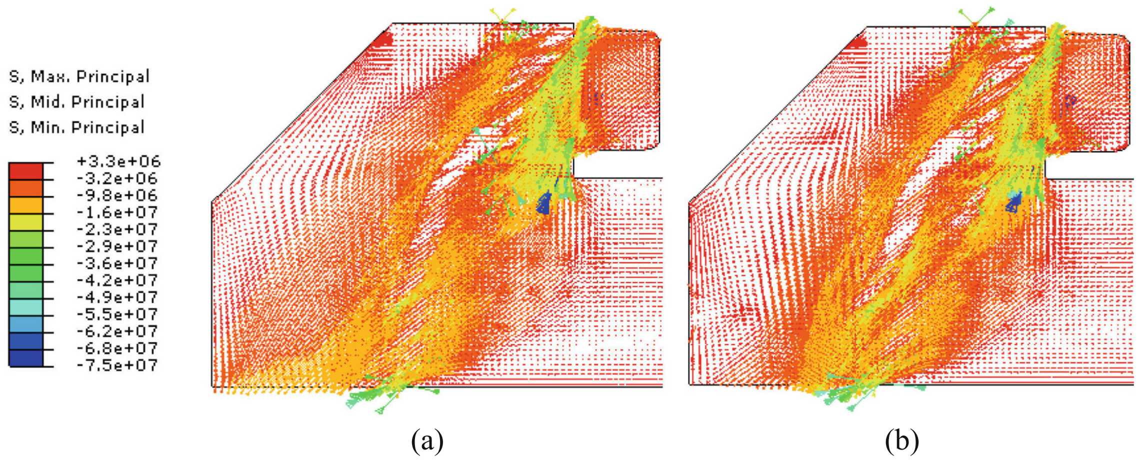

Fig. 7. Tensile stress distribution the slab without steel spirals, as observed at (a) 1 mm or (b) 2 mm of vertical displacement (ABAQUS).

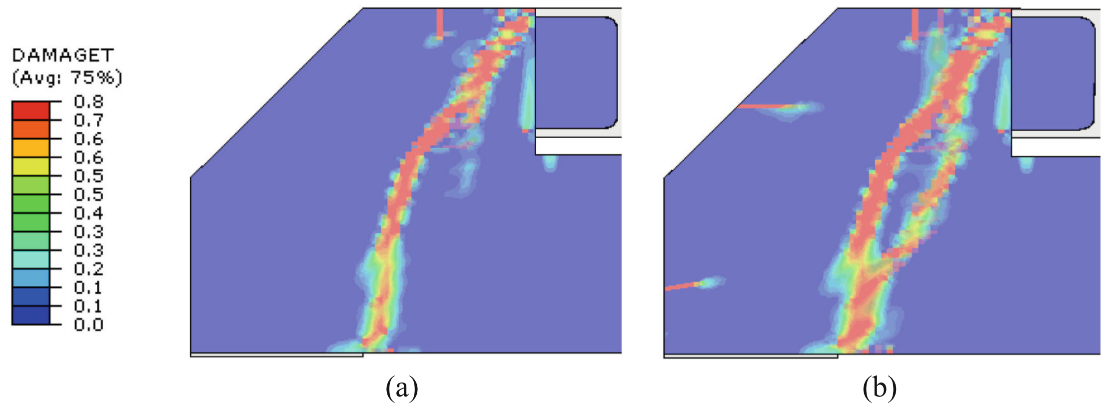

Fig. 8. Tensile damage for the slab without steel spirals, as observed at (a) 1 mm or (b) 2 mm of vertical displacement (ABAQUS).

For comparative purposes, Fig. 9 refers to the slab confined with 2 × 30° spirals, at the same deformation stage. The comparison of contour plots for the unreinforced or confined slab gives clear evidence of the beneficial effect due to spirals.

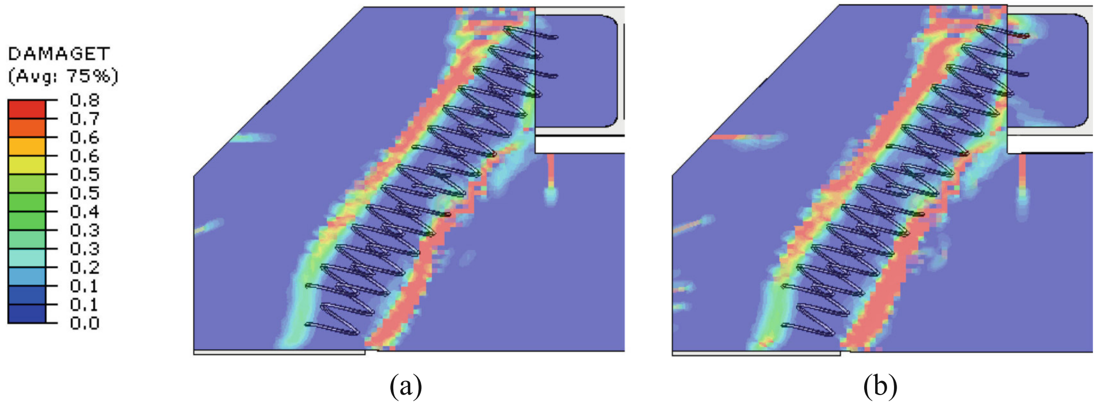

Fig. 9. Tensile damage for the slab with 2 × 30° steel spirals, as observed at (a) 1 mm or (b) 2 mm of vertical displacement (ABAQUS).

In the first case, the propagation of cracks is premature and strongly affect the overall resistance and stiffness parameters of the slab in compression (see also Fig. 6). Conversely, once the steel rebars and spirals are optimally placed to activate an enhanced resisting strut-and-tie mechanism as in Fig. 4, much minor cracks can be observed in the concrete components, with a mostly ductile overall response of the slab that takes the form of a more stable and regular load-displacement characteristic curve.

4 Conclusions

In this paper, the structural performance of reinforced concrete slabs in compression has been explored to maximize the seismic performance of steel-concrete composite frames. As known, the use of spirals can be efficient for the confinement effect of concrete elements, especially with regard to the axial compressive behaviour of columns. At the same time, a multitude of design parameters must be optimally calibrated for the seismic improvement of steel-concrete composite frames. The present study proposed a confinement technique for the slab, based on the use of circular or rectangular steel spirals/fabrics. The final effect is the activation of a strut-and-tie resisting mechanism in which the spirals can interact with the transversal bars in tension. As shown, the optimal arrangement of steel spirals can be extremely beneficial in terms of local and global effects, with marked improvement of post-cracked stiffness, resistance and overall ductility of the slab.

References

1. Marvel L, Doty N, Lindquist W, Hindi R (2014) Axial behavior of high-strength concrete confined with multiple spirals. Eng Struct 60:68–80
2. Sankholkar PP, Pantelides CP, Hales TA (2018) Confinement model for concrete columns reinforced with GFRP spirals. J Compos Constr 22:3
3. Braconi A, Elamary E, Salvatore W (2010) Seismic behaviour of beam-to-column partial-strength joints for steel–concrete composite frames. J Constr Steel Res 66(12):1431–1444

4. Amadio C, Bedon C, Fasan M, Pecce MR (2017) Refined numerical modelling for the structural assessment of steel-concrete composite beam-to-column joints under seismic loads. Eng Struct 138:394–409
5. Amadio C, Bedon C, Fasan M (2017) Numerical assessment of slab-interaction effects on the behaviour of steel-concrete composite joints. J Constr Steel Res 139:397–410
6. Braconi A, Elamary A, Lucchesi D, Salvatore W (2007) Improvement of seismic performances of steel-concrete composite joints by means of slab-column shear connections. In: Proceedings of ANIDIS conference
7. Simulia (2020) ABAQUS computer software, Providence, RI, USA